IEEE Access
Multidisciplinary | Rapid Review | Open Access Journal

Received August 8, 2019, accepted September 2, 2019, date of publication September 9, 2019,
date of current version September 24, 2019.

Digital Object Identifier 10.1109/ACCESS.2019.2940053

Decoupling Control of Maglev Train Based on Feedback Linearization

PENG LENG[1], YAJIAN LI[1], DANFENG ZHOU[1], JIE LI[1], AND SIYANG ZHOU[2]
[1]College of Intelligence Science and Technology, National University of Defense Technology, Changsha 410073, China
[2]Xichang Satellite Launch Center of China, Guiyang 550025, China

Corresponding author: Jie Li (jieli@nudt.edu.cn)

This work was supported by the National Key Research and Development Program of China under Grant 2016YFB1200601.

ABSTRACT The controlled air-gap of the electromagnetic suspension maglev train is generally 8-10 mm, which makes the effect of the vehicle-track dynamic coupling significant. It is found that the track irregularities especially the track step will make the controlled air-gap of the suspension system fluctuate off the setting air-gap. When the situation is even worse, the suspension gap will fluctuate beyond the limit so that the electromagnet or the supporting slide crashes with the track which results in noise and poor ride comfort. By analyzing the gap response of the module suspension system caused by the track step, it is found that the gap fluctuation of the rear point is more significant than the front point. In other words, the suspension gap of the rear point is affected by the front point and the two suspension points couple with each other. To solve the coupling problem between the front and back points, the decoupling controller based on the feedback linearization theory is proposed. The simulation and experiment show that the decoupling controller has an excellent decoupling effect. At the same time, the simulation shows that the decoupling controller can weaken the gap fluctuation when the module suspension system through the track step.

INDEX TERMS Mid-low speed Maglev, track step, fluctuation restrain, decoupling control.

I. INTRODUCTION

The EMS-type urban maglev train uses electromagnetic force to stably suspend the train above the track to achieve non-contact support. Compared with traditional wheel-rail trains, maglev trains have the advantages of small mechanical wear, strong climbing ability, low noise, and small turning radius and so on [1]. The main representatives of EMS-type maglev train are the German Transrapid [2], [3], the Japanese HSST [4], and the Korean UTM [5]. The EMS-type mid-low speed maglev train has been in commercial operation in China after more than 30 years of development [1]. The Changsha Maglev Express Line and the Beijing S1 Line started commercial operation on May 6, 2016 and December 31, 2017 respectively. At the same time, the Qingyuan Maglev tourism special line in Guangdong, as China's third mid-low speed maglev traffic line, began construction in 2018 and was expected to start commissioning by the end of 2019. A number of urban maglev lines are currently being planned [6].

Since the suspension gap of the electromagnetic suspension system is very small, generally 8-10 mm, which results in a limited fluctuation of the controlled air-gap from the equilibrium point. Generally, the gap fluctuation range for the low-speed maglev train is ± 4 *mm* from the equilibrium point, that is, if the equilibrium point is 8 mm, then the gap is allowed to vary within the range of $4 - 12$ *mm*. If air-gap exceeds this range, it is highly probable that the electromagnet or the support slide will crash with the track, generating noise and reducing ride comfort. Such a requirement for the maglev train has made the vehicle-track coupling dynamics problem outstanding. On the one hand, the accuracy of the track must be strictly maintained, which makes the cost of the track relatively high. Generally speaking, the track cost takes up 60%-80% of the initial capital [7]. On the other hand, the smoothness of the track puts forward the requirements to the performance of the suspension control system, and it is necessary to design the corresponding control strategy to obtain better vehicle safety and stability.

Many scholars have done a lot of work in studying the dynamic response of the vehicle-track coupling system for maglev trains in the case of track irregularities.

In [8], aiming at the problem of the maglev train passing over vertical curve and circular curve of the track, Li *et al.* concluded the relationship between the tracking error and

The associate editor coordinating the review of this manuscript and approving it for publication was Ruilong Deng.

FIGURE 1. Beijing S1 Line Maglev Train.

the velocity, the radius of the circular curve, the system control frequency by analyzing the maximum tracking error and the response characteristics of the suspension control system. In [9], Zhao *et al.* developed a 35 degree-of-freedom curving model of the maglev train to analysis its dynamic curving behaviors and concluded that the curve negotiation performance of low-speed maglev train on small radius curves was mainly affected by the vehicle-rail lateral clearance. In [10], Shi *et al.* proposed a new dynamic model of a high-speed EMS maglev vehicle/guideway interaction, considering the vehicle and the guideway as an integral system and the vertical and lateral vehicle/guideway interaction problems. Shi *et al.* further researched on the response of the vehicle-track coupling system in the case of random guideway irregularities. In [11], Pei-Chang *et al.* established a coupling model of the electromagnet module suspension system and the track, further analyzing the effects of the track irregularity such as sleeper spacing, F-track length and beam span. Finally, Yu et al. made some explorations on the suspension control algorithm in the case of considering track smoothness.

Considering the thermal expansion and contraction, the F-track are connected by track joints. Because of the structure of the joint as shown in Figure 3, there is track seam and track step at the track joint. The step at the track joint will cause a large fluctuation in the suspension gap which is generally solved by setting the redundant configuration of the multi-sensor and the related switching fusion algorithm.

Some scholars have done some research on the signal fusion of maglev train sensors. In [12], according to the changing gap signal during the train passed the excessive track gap, Sung *et al.* proposed a model-based fuzzy algorithm which made the system ignore the abnormal gap signal at the joint to weaken the interference to the suspension system. In [13], by analyzing the signal about the suspension gap and the vertical velocity of the electromagnet in different situations, Lin *et al.* proposed a method for correctly identifying the track step to compensate the set gap. That method can restrain the disturbance of railway step effectively. In [14], Zhai and Wu considered the output of the three-probe gap sensor under the condition of track steps and proposed a new gap signal fusion algorithm which weakened the disturbance of the suspension system by the track step. Based on [14], Zhou *et al.* [15] proposed a fusion algorithm for identifying the track step signal and improving the integrated gap signal. The simulation showed that this method can reduce the disturbance of the step signal to the suspension system.

In order to suppress the influence of track irregularity on the system, many scholars have done a lot of research on control algorithms. In [16], Zhang *et al.* introduced the comprehensive acceleration information obtained by using a discrete nonlinear tracking-differentiator to the feedback control and designed a method based on the acceleration to improve the performance of the suspension system. In [17], Zhou proposed the control scheme of positive current feedback and negative acceleration feedback by studying the difference between the measured gap (the gap sensor is installed at the two ends of the electromagnet) and the equivalent gap when the train passed the track step. This method further reduced the interference caused by the track step to the suspension system. In [18], Liu and Zhang proposed a nonlinear feedback algorithm that applied the accelerometer's output and second derivative of the gap to the controls, eliminating the disadvantage brought by the track curve variety. In [19], Zhou *et al.* found that the gap vibration of the rear suspension unit in a suspension module was more significant than that of the front suspension unit and proposed an adaptive vibration control method that utilized the information of the front suspension unit as a reference to suppressing the vibration of the rear suspension gap. In [20], Li *et al.* established a linearized coupled model of the suspension module and the track and proposed a control strategy using the feedback of magnetic flux signals in order to solve the large fluctuation of the rear suspension point.

When the module suspension system passes the track step, the gap response of the rear point is larger than that of the front point [11], [19], [20]. The important reason is that the module suspension system is a two-input and two-output system, and two separately controlled suspension points are coupled. The decoupling problem of module suspension systems has attracted a lot of attention [21]–[23]. These simulations and experiments did not take into account the effects of the track irregularity during actual operation.

By analyzing the gap response of the module suspension system caused by the track step, it is found that the average gap change caused by the track step makes the two suspension points of the module couple with each other, and the gap fluctuation of the rear point is more severe than the front point. A decoupling controller is designed based on the feedback linearization method [32] which can reduce the coupling between the two points of the module suspension system and reduce the gap fluctuation when the module suspension system passes the track step.

The rest of the paper is organized as follows. Section 2 provides the modeling and dynamic analysis of suspension systems. The design of the feedback linearization decoupling controller design is introduced in Section 3 followed by

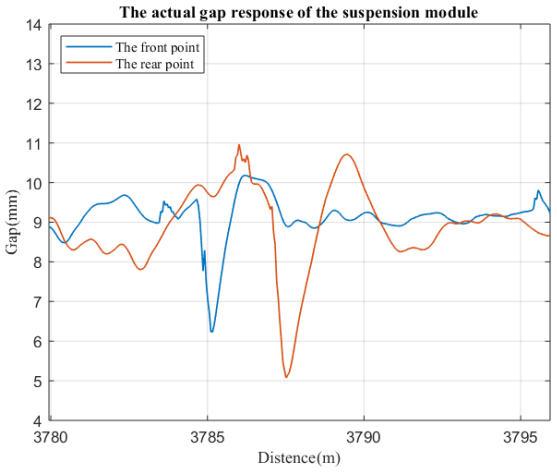

FIGURE 2. The actual gap response of the suspension module's two suspension points through the track II-type joint.

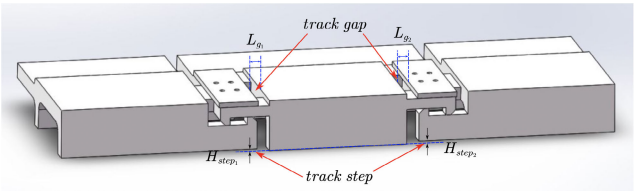

FIGURE 3. The solidworks 3D model of the II-type joint.

simulation analysis and experimental analysis in Section 4. Section 5 summarizes the paper.

II. THE MODEL OF SUSPENSION MODULE SYSTEMS

A. THE ANALYSIS OF TRACK AND SENSORS

The following figure shows the change of the gap about the rear and front point of the suspension module during the actual running of the maglev train in the engineering practice.

It can be seen from the Figure 2 that when the maglev train passed the track's II-type joint, the vertical track irregularities are caused by the seam and the track step at the joint, as shown in Figure 3. When the front and rear points of the suspension module pass through the joint in turn, the suspension gap appears to be offset from the equilibrium point by 9 mm. The gap error of the front point reaches −3mm, and the gap error of the rear point reaches −4mm.

The air-gap sensors are installed on both ends of the electromagnet, so the measured information is only the gap signal at the two ends of the electromagnet (the half-bogie). When the bogie passes over the track steps, if the information measured by the gap sensors is directly regarded as the suspension gap, there is a deviation of 0.66m between the point of the equivalent electromagnetic force and the point at where suspension gap is measured in the case that the length of each suspension module is 1.325m. It can be seen that this measuring method is not accurate.

The equivalent gap refers to the actual air gap between the electromagnet and the track surface. When the electromagnet is regarded as a homogeneous long straight rod, the measuring point is the action point of the equivalent electromagnetic force. When the train is running on the track, the gap of the sensor can truly reflect the equivalent suspension gap of the system in the case that the track is entirely straight. When there exists track step, the equivalent gap of the suspension system is different from the sensor gap because the bogie itself rotates around the center of mass in the xOz plane. The typical process of electromagnet module passing over the track step is shown in Figure 4.

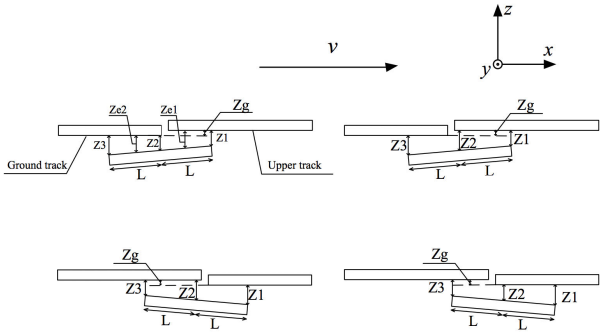

FIGURE 4. The schematic diagram of the equivalent gap of module electromagnet passing over a track step.

Since the width of the track seam is usually 10mm to 45mm, which is much smaller than the length of the electromagnet, the process of the electromagnet passing through the joint gap can be approximated as uniform motion. Based on the lower surface of the track, the height of the joint step is z_g, the forward speed of the electromagnet is v, and the initial time is t_0. The two measured gaps are z_1 and z_3. The half length of the bogie is L. According to the geometric relationship, the air-gap value of the center of mass of the bogie is:

$$z_2 = \frac{z_1 + z_3 - z_g}{2}. \tag{1}$$

When the centroid of the bogie does not pass the track step, the relationship between the measured gap and the equivalent gap is:

$$\begin{cases} z_{e1} = \dfrac{3z_1 + z_3 - 3z_g}{4} + \dfrac{z_g v(t - t_0)}{L}, \\ z_{e2} = \dfrac{z_1 + 3z_3 - z_g}{4}. \end{cases} \tag{2}$$

After the center of bogie passes through the step, the equivalent gap is derived from the geometrical relationship:

$$z_2 = \frac{z_1 + z_3 - z_g}{2} + z_g. \tag{3}$$

The relationship between the gap measured by the sensor and the equivalent gap is:

$$\begin{cases} z_{e1} = \dfrac{3z_1 + z_3 + z_g}{4}, \\ z_{e2} = \dfrac{z_1 + 3z_3 - z_g}{4}. \end{cases} \tag{4}$$

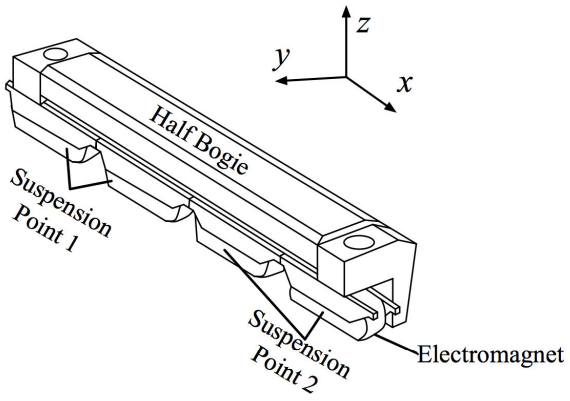

FIGURE 5. The half-bogie cabinet axonometric projection.

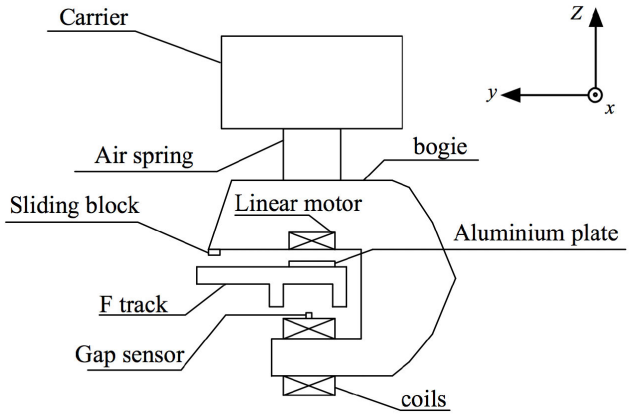

FIGURE 6. The half-bogie view of the x-direction.

According to the above derivation, we obtain the equivalent gap of the suspension system and use it to calculate the electromagnetic force.

B. MATHEMATICAL MODEL

The half bogie of the mid-low speed maglev train is rigidly connected. And the module is divided into two suspension points, as shown in Figure 5. Each point contains two electromagnets. The suspension force is controlled by controlling the current of two suspension points [24]. The cross-section of this module is shown in Figure 6.

Since the bogie is equipped with a transverse tie rod, the electromagnet is constrained in the y-direction, and its rolling movement is also limited because of the presence of the anti-roll beam. Therefore, the movement of the electromagnet in the y-axis direction can be neglected in the case of establishing the double-point suspension model. The complexity of the model is reduced because only the translation of the x-axes and z-axes and the pitching motion around the y-axis are considered.

1) OPEN-LOOP MODEL OF THE MODULE SUSPENSION SYSTEM

Firstly, the certain assumptions about the suspension module system are made as follows [25]:

1. Winding leakage magnetic flux is ignored;
2. The magnetic resistance of the iron core and the guide rail is ignored;
3. The track is regarded as a rigid track, regardless of its elastic coupling vibration. That is to say that the stiffness coefficient of the track relative to the electromagnet is considered to be infinite
4. It is assumed that the mass of the suspension module is evenly distributed, and the whole side of the module is a straight rod with uniform mass distribution. The centroid of the straight rod coincides with the geometric center. The suspension module is divided into two single suspension points that are coupled to each other.
5. The electromagnetic force at the front and rear points is regarded as a concentrated force, acting on the geometric center of the front and rear points.

The above five simplified assumptions can be concluded by finite element analysis [26]: the error of the calculation result under the above conditions will not exceed 10%, which meets the engineering requirements.

Let $k = \frac{\mu_0 N^2 A}{4}$, Then the following mathematical model (μ_0 is the permeability of vacuum) is established.

a: VOLTAGE-CURRENT EQUATION

Air gap flux in the case of ignoring core reluctance:

$$\phi = \frac{F}{R_{gap}} = \frac{Ni(t)}{2z(t)/(\mu_0 A)}. \tag{5}$$

Air gap flux linkage:

$$\psi = N\phi. \tag{6}$$

According to the electromagnetic equation, the voltage balance equation can be deduced as:

$$\begin{aligned} u_1 &= R_1 i_1(t) + \frac{d\psi_1}{dt} \approx R_1 i_1(t) + \frac{d}{dt}\left(\frac{N^2 i_1(t)\mu_0 A}{2Z_1(t)}\right) \\ &= R_1 i_1(t) + \frac{N^2\mu_0 A}{2Z_1(t)}\frac{di_1(t)}{dt} - \frac{N^2\mu_0 A i_1(t)}{2Z_1^2(t)}\frac{dZ_1(t)}{dt}. \end{aligned} \tag{7}$$

$$\begin{aligned} u_2 &= R_2 i_2(t) + \frac{d\psi_2}{dt} \approx R_2 i_2(t) + \frac{d}{dt}\left(\frac{N^2 i_2(t)\mu_0 A}{2Z_2(t)}\right) \\ &= R_2 i_2(t) + \frac{N^2\mu_0 A}{2Z_2(t)}\frac{di_2(t)}{dt} - \frac{N^2\mu_0 A i_2(t)}{2Z_2^2(t)}\frac{dZ_2(t)}{dt}. \end{aligned} \tag{8}$$

b: ELECTROMAGNETIC FORCE EQUATION

In the case where the electromagnet has no magnetic flux leakage, the magnetic field energy storage is $w_{fld} = \frac{1}{2}L(z)i^2$ and its inductance is $L(z) = \frac{\mu_0 N^2 A}{2z}$. Magnetic field energy storage is a state function that is uniquely determined by independent variables z (displacement) and ψ (magnetic flux).

According to the partial differential equation $F = -\frac{\partial W_{fld}}{\partial z}|\psi = const$, it can be obtained that:

$$\begin{cases} F_{e1}(i_1, z_1) = \dfrac{\mu_0 N^2 A}{4}\left(\dfrac{i_1(t)}{z_1(t)}\right)^2, \\ F_{e2}(i_2, z_2) = \dfrac{\mu_0 N^2 A}{4}\left(\dfrac{i_2(t)}{z_2(t)}\right)^2. \end{cases} \tag{9}$$

c: CENTROID KINETIC EQUATION

The suspension module system can be regarded as a rigid body point system. The displacement of the centroid in the z-axis direction is:

$$z = \frac{z_{e1}(t) + z_{e2}(t)}{2}. \tag{10}$$

Centroid acceleration of the half bogie:

$$a_c = \frac{d^2}{dt^2}(z(t)) = \frac{d^2}{dt^2}\left(\frac{z_{e1}(t) + z_{e2}(t)}{2}\right). \tag{11}$$

From the above, it has

$$2ma_c = 2m\frac{d^2}{dt^2}(z(t)) = 2m\frac{d^2}{dt^2}\left(\frac{z_{e1}(t) + z_{e2}(t)}{2}\right). \tag{12}$$

where m is the mass of a single electromagnet module and M is the mass of the body of the vehicle. When the system is to be in a state of equilibrium, there are:

$$F_{e10} = F_{e20} = \frac{(2m + M)g}{2}. \tag{13}$$

d: CENTROID MOMENT EQUATION

The moment of inertia and angular acceleration of the suspension module around the centroid are respectively J_c and $\frac{d\omega}{dt}$. According to the centroid moment equation, it has:

$$J_c\frac{d\omega}{dt} = \sum M_c\left(F_i^{(e)}\right). \tag{14}$$

When the fluctuations of the two suspension points are inconsistent, the bogie will not only be moving vertically in the z-axis direction but also roll around the centroid in the xOz plane. If the direction of counterclockwise rotation is the positive direction, the moment of inertia and angular acceleration of the suspension module around the centroid can be obtained.

$$\begin{cases} J_c = \dfrac{1}{12}(2m)(2l)^2 = \dfrac{2}{3}ml^2, \\ \dfrac{d\omega}{dt} = \dfrac{d}{dt}((\dot{z}_1(t) - \dot{z}_2(t))\backslash(l/2) = \dfrac{2}{l}((\ddot{z}_1(t) - \ddot{z}_2(t)). \end{cases} \tag{15}$$

Since the gravity acts to the centroid of the module, the moment caused by gravity:

$$M_c[(2m + M)g] = 0. \tag{16}$$

The torque of electromagnetic force:

$$M_c\left(F_{e1}, F_{e2}\right) = \frac{l}{2}\left(F_{e1} - F_{e2}\right). \tag{17}$$

From the moment of momentum equation, it has:

$$\frac{8}{3}m\left(\dot{z}_1(t) - \dot{z}_2(t)\right) = F_{e1} - F_{e2}. \tag{18}$$

The meaning of each variable in the above equations is shown in the following table:

In summary, let $X = [x_1, x_2, x_3, x_4, x_5, x_6]^T = [z_1(t), z_2(t), \dot{z}_1(t), \dot{z}_2(t), i_1(t), i_2(t)]^T$, $R_1 = R_2 = R$. The

TABLE 1. Variables in the above equation.

Variable	Description
m	Single point bearing quality under spring
M	Single point bearing quality above the spring
ϕ	Air gap flux
l	The length of the single electromagnet module
ψ	Air gap flux linkage
z_1	The suspension gap in point 1
z_2	The suspension gap in point 2
N	Winding turns
i_1	The electromagnet current in point 1
i_2	The electromagnet current in point 2
A	Core area of electromagnet
R	Magnetic circuit reluctance

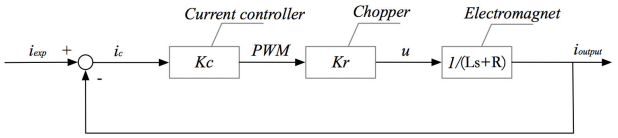

FIGURE 7. The current loop diagram.

mathematical model of the double electromagnet suspension system can be obtained:

$$\begin{cases} \dot{x}_1 = x_3, \\ \dot{x}_2 = x_4, \\ \dot{x}_3 = \dfrac{2m + M}{2m}g - \dfrac{5k}{4m}\left(\dfrac{x_5}{x_1}\right)^2 + \dfrac{k}{4m}\left(\dfrac{x_6}{x_2}\right)^2, \\ \dot{x}_4 = \dfrac{2m + M}{2m}g - \dfrac{5k}{4m}\left(\dfrac{x_6}{x_2}\right)^2 + \dfrac{k}{4m}\left(\dfrac{x_5}{x_1}\right)^2, \\ \dot{x}_5 = \dfrac{x_1}{2k}u_1 - \dfrac{x_1x_5}{2k}R + \dfrac{x_3x_5}{x_1}, \\ \dot{x}_6 = \dfrac{x_2}{2k}u_1 - \dfrac{x_2x_6}{2k}R + \dfrac{x_4x_6}{x_2}. \end{cases} \tag{19}$$

2) TRADITIONAL CONTROL SCHEME

For the unstable suspension module system, the dual-loop PID control which includes the current loop and the position loop is used [27]. The voltage-current equation in the model is subjected to a Laplace transform. The transfer function is:

$$\frac{i(s)}{u(s)} = \frac{1}{R(s) + s\left(\frac{\mu_0N^2A}{2z}\right) - \left(\frac{\mu_0N^2A\dot{z}}{2z^2}\right)} = \frac{1}{R'(s) + sL'(s)}. \tag{20}$$

In the actual system, due to the existence of the inductance, the current cannot respond quickly to the change of the voltage, so that the response of the suspension system is delayed. The system's delay can be effectively reduced by introducing the current loop. The control flow graph is shown in Figure 7.

The closed-loop transfer function of the current loop is:

$$G_{ic}(s) = \frac{K_cK_r}{sL'(s) + R'(s) + K_cK_r}. \tag{21}$$

There is $G_ic \approx 1$ in the case of $K_cK_r >> R'$ and $K_cK_r >> L'$, and the current loop can be regarded as a proportional link with a gain of about 1.

Introduce feedback vectors $K = [K_p, K_d, K_i]$ in the case where the gain of the current loop is approximately 1. The position loop control rate is:

$$i_{exp} = K_p\Delta z + K_d\Delta\dot{z} + K_i\int \Delta z dt. \tag{22}$$

III. STEP INTERFERENCE ANALYSIS BASED ON DECOUPLING CONTROL

Based on the model of the suspension module system, the feedback linearization decoupling method is used to decouple the nonlinear module suspension system into two independent SISO systems.

A. FEEDBACK LINEARIZATION THEORY

A general nonlinear system can be represented by the following equation:

$$\sum : \begin{cases} \dot{x} = f(x) + g(x)u \quad x(t_0) = x_0, \\ y = h(x, u). \end{cases} \tag{23}$$

where: $x \in M \subset R^n$ is the state vector, $x \in R^m$ is the output vector, $y \in R^r$ is the output vector, f and h is the analytic function vector of the independent variable about x and u.

The following theorem can be used to judge the decoupling of the system [28].

Theorem 1: For a given system, the following three propositions are true:

1. The relative order of the system $\sum : \alpha(\Sigma) \le n$.
2. The system $\sum$ is controllable (reversible)
3. The system $\sum$ can be transformed into an integral decoupling system under state feedback and dynamic compensation conditions.

If a MIMO system is decoupled according to the above theorem, the following decoupling control algorithm can be used for control:

1. Solve its α-order integral inverse system from the equation of state of the original system.
2. The original system is compensated according to the solved α-order integral inverse system, which is transformed into a standard integral decoupling system conforming to the definition in this section.
3. The subsystems of the decoupled system are regarded as controlled objects. The appropriate poles are configured according to predetermined performance indicators, so that the performance of each subsystem meets the expected requirements.

B. DECOUPLING CONTROLLER DESIGN

The model of the suspension module is rewritten as:

$$\begin{cases} \dot{x} = f(x) + g(x)u, \\ y = h(x, u) \quad x(t_0) = x_0. \end{cases} \tag{24}$$

where

$$f(x) = \begin{bmatrix} x_3 \\ x_4 \\ \frac{2m+M}{2m}g - \frac{5k}{4m}(\frac{x_5}{x_1})^2 + \frac{k}{4m}(\frac{x_6}{x_2})^2 \\ \frac{2m+M}{2m}g - \frac{5k}{4m}(\frac{x_6}{x_2})^2 + \frac{k}{4m}(\frac{x_5}{x_1})^2 \\ -\frac{x_1x_5}{2k}R + \frac{x_3x_5}{x_1} \\ -\frac{x_2x_6}{2k}R + \frac{x_4x_6}{x_2} \end{bmatrix}. \tag{25}$$

$$g(x) = \begin{bmatrix} 0 & 0 \\ 0 & 0 \\ 0 & 0 \\ 0 & 0 \\ \frac{x_1}{2k} & 0 \\ 0 & \frac{x_2}{2k} \end{bmatrix} \quad u = \begin{bmatrix} u_1 & u_2 \end{bmatrix}. \tag{26}$$

$$h(x) = \begin{bmatrix} h_1(x) \\ h_2(x) \end{bmatrix} = \begin{bmatrix} x_1 \\ x_2 \end{bmatrix}. \tag{27}$$

According to the *Lie* derivative [29], [33], the output of the suspension system is derived as follows:

The rear point of the suspension module:

$$\begin{cases} L_f^0 h_1(x) = x_1, \\ L_{g1}L_f^0 h_1(x) = 0, \\ L_{g2}L_f^0 h_1(x) = 0, \\ L_f h_1(x) = x_3, \\ L_{g1}L_f h_1(x) = 0, \\ L_{g2}L_f h_1(x) = 0, \\ L_f^2 h_1(x) = -\frac{5k}{4m}(\frac{x_5}{x_1})^2 + \frac{k}{4m}(\frac{x_6}{x_2})^2 + \frac{2m+M}{2m}g, \\ L_{g1}L_f^2 h_1(x) = -\frac{5x_5}{4mx_1}, \\ L_{g2}L_f^2 h_1(x) = \frac{x_6}{4mx_2}, \\ L_f^3 h_1(x) = \frac{5x_5^2R}{4mx_1} - \frac{x_6^2R}{4mx_2}. \end{cases} \tag{28}$$

The front point of the floating module:

$$\begin{cases} L_f^0 h_2(x) = x_2, \\ L_{g1}L_f^0 h_2(x) = 0, \\ L_{g2}L_f^0 h_2(x) = 0, \\ L_f h_2(x) = x_2, \\ L_{g1}L_f h_2(x) = 0, \\ L_{g2}L_f h_2(x) = 0, \\ L_f^2 h_2(x) = -\frac{5k}{4m}(\frac{x_6}{x_2})^2 + \frac{k}{4m}(\frac{x_5}{x_1})^2 + \frac{2m+M}{2m}g, \\ L_{g1}L_f^2 h_2(x) = \frac{5x_5}{4mx_1}, \\ L_{g2}L_f^2 h_2(x) = -\frac{5x_6}{4mx_2}, \\ L_f^3 h_2(x) = -\frac{x_5^2R}{4mx_1} + \frac{5x_6^2R}{4mx_2}. \end{cases} \tag{29}$$

From the above derivation, it has $L_{gj}L_f^2 h_1(x_0) \neq 0$ at the equilibrium point of the suspension system for the first

output $h_1(x)$. Similarly, for the second output $h_2(x)$, the derivation is similar, namely $L_{gj}L_f^2h_2(x_0) \neq 0$.

Therefore, the relative order vector of the suspension system is $[r_1(x_0), r_2(x_0)] = [3, 3]$, which satisfies $r_1(x_0) + r_2(x_0) \leq n$. Therefore, according to Theorem 1, the system is decouplable and can be converted into an integral decoupling system by state feedback and dynamic compensation.

The decoupling matrix:

$$E = \begin{bmatrix} L_{g1}L_f^2h_1(x) & L_{g2}L_f^2h_1(x) \\ L_{g1}L^2f_2(x) & L_{g2}L_f^2h_2(x) \end{bmatrix} = \begin{bmatrix} -\dfrac{5x_5}{4mx_1} & \dfrac{x_6}{4mx_2} \\ \dfrac{x_5}{4mx_1} & -\dfrac{5x_6}{4mx_2} \end{bmatrix}. \tag{30}$$

This decoupling matrix is non-singular, so you can set the feedback control rate $u = E^{-1}(x)[-b(x) + v]$, where

$$b(x) = \begin{bmatrix} L_f^3h_1(x) & L_f^3h_2(x) \end{bmatrix}^T = \begin{bmatrix} \dfrac{5x_5^2R}{4mx_1} - \dfrac{x_6^2R}{4mx_2} & \dfrac{-x_5^2R}{4mx_1} + \dfrac{5x_6^2R}{4mx_2} \end{bmatrix}^T. \tag{31}$$

Let $\ddot{y} = \varphi$, find the functions u_1 and u_2 :

$$u = \begin{bmatrix} x_5R - \dfrac{(5\varphi_1 + \varphi_2)\, mx_1}{6x_5} & x_6R - \dfrac{(5\varphi_2 + \varphi_1)\, mx_2}{6x_6} \end{bmatrix}^T. \tag{32}$$

where x_1, x_2 are the measured gap of the front suspension point and the rear suspension point respectively. x_5 and x_6 are the current through the front and rear coil pair respectively.

After that, the two subsystems become two independent 3-order integral systems. The state variable of the first integral system is $z = \begin{bmatrix} x_1 & \dot{x}_1 & \ddot{x}_1 \end{bmatrix}$, and the input variable is $v = \varphi_1$. The state variable of the first second integral system is $z = \begin{bmatrix} x_2 & \dot{x}_2 & \ddot{x}_2 \end{bmatrix}$, and the input variable is $v = \varphi_2$. Then both integral systems can be represented by the following state equation:

$$\begin{cases} \dot{z} = Az + Bv \\ y = Cz. \end{cases} \tag{33}$$

where:

$$A = \begin{bmatrix} 0 & 1 & 0 \\ 0 & 0 & 1 \\ 0 & 0 & 0 \end{bmatrix}, \quad B = \begin{bmatrix} 0 \\ 0 \\ 1 \end{bmatrix}, \quad C = \begin{bmatrix} 1 & 0 & 0 \end{bmatrix}.$$

The rank of the controllability matrix:

$$\text{Rank}\,(R_c) = \text{Rank}\left(\begin{bmatrix} B & AB & A^2B \end{bmatrix}\right) = 3. \tag{34}$$

Based on the above calculation, the system is entirely controllable.

The feedback control law is designed for (33).

$$v = -\left(kz + v_{ref}\right). \tag{35}$$

where $v_{ref} = \begin{pmatrix} \mathbf{z}_{ref} & 0 & 0 \end{pmatrix}^T$.

Substituting the feedback control law into the integral system obtains the characteristic equation of the closed-loop system.

$$s^3 + k_3s^2 + k_2s + k_1 = 0. \tag{36}$$

Set the following system performance indicators:

1. System overshoot: $\sigma \leq 5\%$;
2. The time when the system rises to the peak: $t_\sigma < 0.1s$;

It has:

$$\begin{cases} \sigma = e^{-\zeta\pi/\sqrt{1-\zeta^2}} \leq 5\%, \\ t_\sigma = \pi/(\omega_n\sqrt{1-\zeta^2}) \leq 0.1. \end{cases} \tag{37}$$

The solution of (37) is $\xi \geq 0.69$ and $\omega_n \geq 43.4$. Let $\zeta = 0.707$, so the expected dominant pole is $s_{1,2} = -40 \pm 40j$. According to the principle of pole placement, the distance between the non-dominant pole and the imaginary axis is ten times that of the dominant pole, so the third pole is taken as $s_3 = -400$.

According to the pole, the characteristic equation of the third-order pure integral system can be obtained:

$$s^3 + 480s^2 + 64000s + 1280000 = 0. \tag{38}$$

Therefore, the input variable in the finalized inverse system is:

$$\varphi = -1280000\left(z_1 - z_{ref}\right) - 64000z_2 - 480z_3. \tag{39}$$

C. STABILIZATION OF DECOUPLING SYSTEMS

The feedback linearization in this paper is based on the inverse system method to transform the original system into a pseudo linear system, and then the system is dynamically integrated. Moreover, the model in this paper is far complicated. It is quite complicated to directly analyze the complete stabilization of the decoupling system. The conclusion can be drawn from the analysis of the pseudo linear system structure. The state equation for a pseudo linear system is generally expressed as [30]:

$$\begin{cases} \dot{z}_j = A_jz_j + B_jv_j \quad j \in \underline{q}, \\ \dot{x} = f(x, \phi(x, z, v)), \\ y = h(x, \phi(x, z, v)). \end{cases} \tag{40}$$

where $x = (x_1, x_2, \cdots, x_n)^T \in R^n$ represents the state variable of the system, $v = \left(v_1, v_2, \cdots, v_q\right)^T = \left(y_1^{(n_{e1})}, y_2^{(n_{22})}, \cdots, y_q^{(n_{aq})}\right)^T$ is the input vector of the pseudo linear system, n_{ej} is the natural order of the output y_j ($j \in \underline{q}$), $y = \left(y_1, y_2, \cdots, y_q\right)^T \in R^q$ represents the output vector of the system, $z = \left(z_1, z_2, \cdots, z_q\right)^T$ indicates the state variable of the decoupled system, each component is $z_j = \left(z_{j1}, z_{j2}, \cdots, z_{j\lambda_j}\right)^T$ ($\lambda_j = n_{ej} - \alpha_j$), α_j is the relative order vector of the system.

Therefore, the internal variable of the pseudo linear composite system is $(z^T, x^T)^T$, the dimension of $(z^T, x^T)^T$ is $n + \dim(z) = \sum_{j=1}^{q} n_{ej} - \sum_{j=1}^{q} \alpha + n$. For the pseudo linear

system described above, the following state transitions can be constructed:

$$\begin{cases} x^* = x^*(x, z), \\ z^* = z^*(x, z). \end{cases} \tag{41}$$

According to the paper [31], by the inverse function theorem, there is an inverse function:

$$\begin{cases} x = x(x^*, z^*), \\ z = z(x^*, z^*). \end{cases} \tag{42}$$

where the dimensions of x^* and z^* are $\dim(x^*) = n + \dim(z) - \sum_{j=1}^{q} n_{ej} = n - \sum_{j=1}^{q} \alpha_j$ and $\dim(x^*) = \sum_{j=1}^{q} n_{ej}$ respectively.

Substituting (42) into (40) for state transformation, it can be proved that the transformed system can be expressed as:

$$\begin{cases} \dot{z}_j^* = A_j^* z_j^* + B_j^* v_j^* \quad j \in \underline{q}, \\ \dot{x}^* = f^*\left(x^*, z^*, v\right)), \\ y = C^* z^*. \end{cases} \tag{43}$$

Equation (43) shows that the state equation of the pseudo linear composite system can be decomposed into two parts: the linear part and the nonlinear part. The first and third equations in equation (43) are linear part, which is counted as subsystem Σ_1 and is a controllable and observable system. The second formula in equation (43) is a nonlinear part, which is counted as a subsystem Σ_2 and is an unobservable system.

Since Σ_1 is controllable, it can always be robust stability by full state feedback. Therefore, whether or not a stable decoupling system can be obtained will depend entirely on whether the subsystem Σ_2 is stable. It is pointed out in the paper [31] that $\dim(x^*) = 0$ is obtained in the case of $\sum_{j=1}^{q} \alpha_j = n$, so the second formula in equation (43) is 0 and the nonlinear system can be completely linearized. In other word, the pseudo linear composite system does not contain the nonlinear part. As long as the linear part is guaranteed to be robust stability, the whole system is robust stability.

According to the analysis of the DECOUPLING CONTROLLER DESIGN, the relative order of the suspension system is $\sum_{j=1}^{q} \alpha_j = 3+3 = 6$ and n in the suspension system is 6. This is very obvious that the formula $\sum_{j=1}^{q} \alpha_j = n$ is established. From the above argument, the suspension system in this paper can be completely linearized. According to the Lyapunov method [28], for the linear time-invariant systems, every equilibrium state of the system is stable in the sense of Lyapunov if and only if all the eigenvalues of system matrix have non-positive (negative or zero) real parts and the eigenvalues of zero real parts are single roots of the smallest polynomial. And for the linearized subsystem, the eigenvalues of the system matrix in the closed loop subsystem all have a negative real part, so the subsystem is progressively stable. At the same time, according to Chapter 13 of literature [28], the closed-loop system has certain robust stability to model uncertainty by the Lyapunov analysis. So, from the above argument, the entire nonlinear suspension system can also guarantee robust stability.

IV. SIMULATION AND EXPERIMENT

In order to evaluate the performance of the proposed decoupling control, the simulation and the half bogie maglev platform were used for testing. The suspension module system has suspension point 1 and suspension point 2, as shown in Figure5.

The simulation is based on the suspension module system, and the parameters are determined by the actual maglev train. The sampling and control frequency is set to $4000Hz$ in the program. In the simulation test, the shape and related parameters of the II-type joint are shown in Figure 3.

A. SIMULATION RESULTS

The simulation parameters are shown in Table 2. The 'track gap' in Table 2 is the clearance of the track joint, as shown in Figure 3.

TABLE 2. Parameters in the Simulation.

Variable	Description	Value
m	Single point bearing quality under spring	$500Kg$
M	Single point bearing quality above the spring	$1300Kg$
l	The length of single electromagnet module	$1.3m$
Track	The length of the track	$109m$
Step	The height of the step	$2.7mm$
Track gap	The clearance of the track joint	$40mm$
k_p	The proportional parameter of PID algorithm	4500
k_i	The integral parameter of PID algorithm	950
k_d	The differential parameters of PID algorithm	4
k_c	The current loop gain	200
Speed	The speed of train	$5m/s$

According to the forward direction of the suspension module, we set the suspension point 2 as the front point and the suspension point 1 as the rear point, as shown in Figure 5. The module system continuously passes through two track steps, which are respectively 2.7mm upper step and 2.7mm lower step. The simulation results of the PID algorithm and decoupling control algorithm are shown in Figure 8 and Figure 9.

According to the data from Figure 8 and Figure 9, when the system adopts the PID algorithm, the maximum suspension gap error of the rear point is 4.3*mm* and the maximum suspension gap error of the front point is 3.847*mm* under the case of the equilibrium point of 9*mm*. When the system adopts decoupling control algorithm, the maximum suspension gap error of the rear point is 3.855*mm* and the maximum suspension gap error of the front point is 3.774*mm* under the case of the equilibrium point of 9*mm*. So, the fluctuations of the front and rear points are obtained, as shown in Table 3.

By comparing the simulation results of Figure 8 and Figure 9, it can be seen that when the suspension system adopts the decoupling control algorithm, the maximum suspension gap error of the front and rear points becomes smaller. In other words, the degree of coupling between the

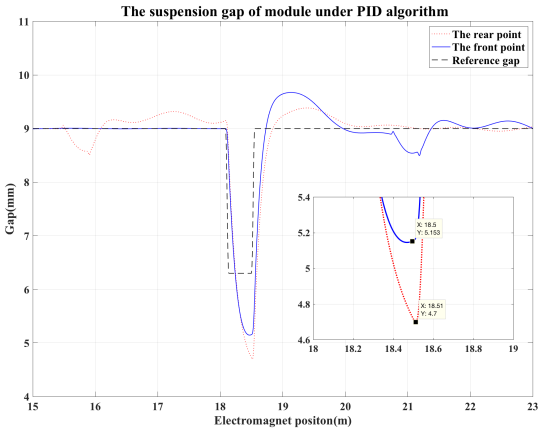

FIGURE 8. The suspension gap of the module using the PID algorithm.

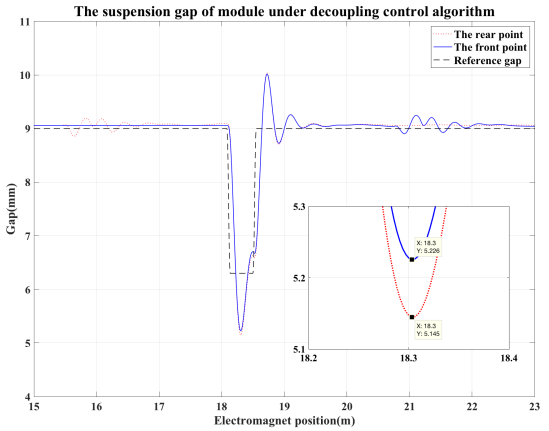

FIGURE 9. The suspension gap of the module using the decoupling control algorithm.

TABLE 3. The maximum suspension gap error of two algorithms in simulation.

	PID	Decoupling Control	Reduction
The rear point	$4.3mm$	$3.855mm$	10.35%
The front point	$3.847mm$	$3.774mm$	1.9%

front and back points is reduced. Therefore, the decoupling control algorithm is more effective than the PID control when the module passes through the track step.

B. EXPERIMENTAL RESULTS

This paper takes the small-scale half bogie experimental platform developed by the Magnetic Suspension Center of National University of Defense Technology as the experimental object, as shown in Figure 10. The parameters of the platform are summarized in Table 4.

Experiment scheme: After the platform is stably suspended, the front point (the suspension point 1) is set to track a square wave with an amplitude of $0.5mm$ and a frequency

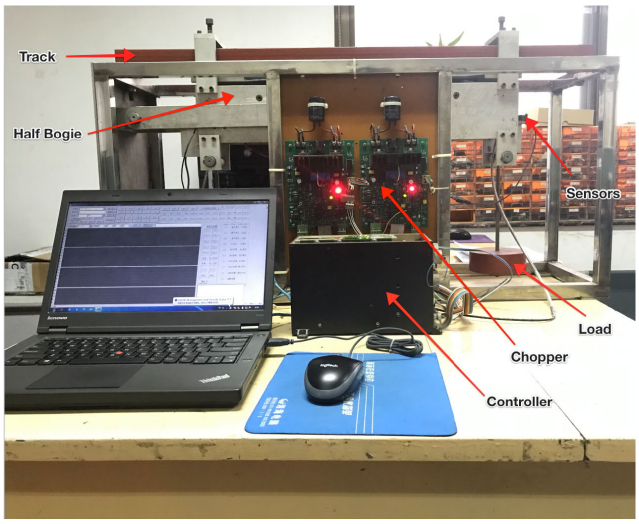

FIGURE 10. The small-scale half bogie experiment platform.

TABLE 4. The parameters of the small-scale half bogie experiment platform.

Parameters	Description	Value
μ_0	Permeability of vacuum	$4\pi \times 10^{-7} N \cdot A^{-2}$
g	Accelerate of gravity	$9.81m \cdot s^{-2}$
A	The effective area of per electromagnet	$0.0014m^2$
N	Coil turns number of per electromagnet	540
R	Coil resistance of per electromagnet	2.1Ω
L	Length of a bogie	$0.65m$
m	Mass of a bogie	$5.2Kg$
M	Mass of load	$16Kg$

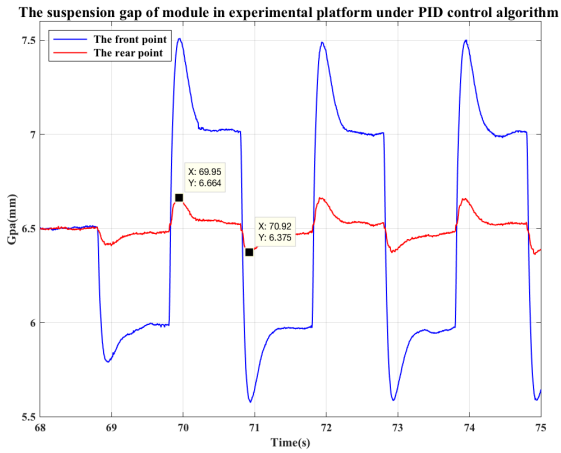

FIGURE 11. The suspension gap of the module in the experimental platform with PID algorithm.

of $0.5Hz$ which observes the control effect of the decoupling algorithm and the PID control algorithm.

For the suspension system, a fast response to track disturbances is critical to good dynamic performance, which means less overshoot, fewer fluctuations and shorter transition times for the system. Therefore, this paper evaluates the system

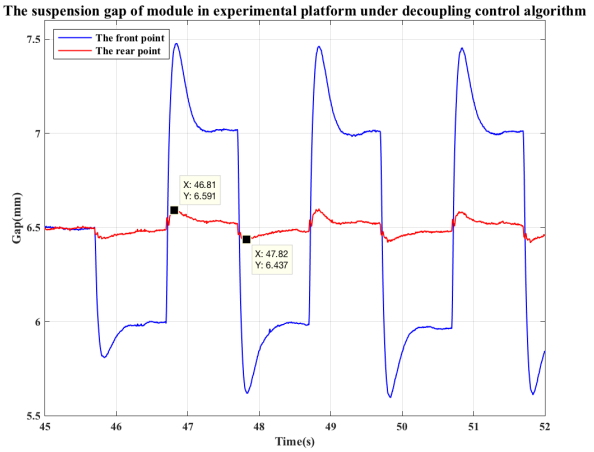

FIGURE 12. The suspension gap of the module in the experimental platform under decoupling control algorithm.

TABLE 5. The ITAE of the suspension gap at the front and rear point under the two algorithms.

	PID	Decoupling Control	Reduction
The rear point	0.1949	0.1683	13.65%
The front point	0.0937	0.0732	21.88%

TABLE 6. The maximum suspension gap error of the rear point under two algorithms in the experiment.

	PID	Decoupling Control	Fluctuation Reduction
At the rising edge of the step	$0.164mm$	$0.091mm$	44.5%
At the falling edge of the step	$0.125mm$	$0.063mm$	49.6%

performance of the control system by calculating the integral of the time-weighted absolute error. The integral of the time-weighted absolute error [ITAE] is defined as

$$ITAE = \int_0^\infty t|e(t)|dt. \tag{44}$$

The time span selected when calculating the ITAE is one period of the square wave applied to the front point. The ITAE calculation result is shown in Table 5.

According to the data from Figure 11 and Figure 12, when the system adopts the PID algorithm, the suspension gap at the rising edge of the step is 6.664mm and the suspension gap at the falling edge of the step is 6.375mm. When the system adopts the decoupling control algorithm, the suspension gap at the rising edge of the step is 6.591mm and the suspension gap at the falling edge of the step is 6.437mm. Therefore, the suspension gap error of the front and rear points under the case of the equilibrium point of 6.5mm is obtained, as shown in Table 6.

According to the experimental data, compared with the PID algorithm, when the decoupling control algorithm is adopted in the suspension system and the disturbance is received at one point, the suspension gap error of the other point is reduced by a maximum of 49.6%. ITAE indicators focus on assessing system transition times and fluctuations, which reflects the ability of the system to operate stably over the long term. So, From the results of ITAE in Table 5, it can be seen that the system adopted the decoupling control algorithm has a great improvement in transition time and fluctuation. It is verified that the decoupling control algorithm can effectively solve the control problem when two points are coupled to each other. At the same time, the decoupling control algorithm needs further experimental verification on the running medium speed vehicle.

V. CONCLUSION

In this paper, based on the engineering reality that the suspension system fluctuates too much when the low-speed maglev train passes over the track steps, the fluctuation of the gap when the maglev train passed over the step is analyzed. Based on the module suspension system, the decoupling control algorithm based on the feedback linearization is proposed. By adopting the decoupling control algorithm based on feedback linearization, the mutual influence of the two mutual coupling points is effectively solved, further enhancing the passenger's ride comfort. Both simulation and experiment prove that after the improved method, the impact of the step on the suspension system is reduced, and the suspension performance is further improved. Simulation and experimental results verify the effectiveness of the improved method. And the next step is to go to the Tangshan test line to conduct relevant experiments to further verify the effectiveness of the proposed method.

REFERENCES

[1] L. Yan, "Development and application of the maglev transportation system," *IEEE Trans. Appl. Supercond.*, vol. 18, no. 2, pp. 92–99, Jun. 2008.
[2] B. Sands, "The German magnetic levitation train (transrapid)," *Built Environ.*, vol. 19, no. 3, p. 244, 1993.
[3] G. Wahl, "The maglev system transrapid—A future-orientated technology for track-bound transportation systems," in *Proc. 18th Int. Conf. Magn. Levitated Syst. Linear Drives*, 2004, p. 32.
[4] Y. Yasuda, M. Fujino, M. Tanaka, and S. Ishimoto, "The first HSST maglev commercial train in Japan," in *Proc. 18th Int. Conf. Magn. Levitated Syst. Linear Drives (MAGLEV)*, 2004, pp. 76–85.
[5] N. Lee, H. Han, J. Lee, and B. Kang, "Maglev vehicle/guideway dynamic interaction based on vibrational experiment," in *Proc. Int. Conf. Electr. Mach. Syst. (ICEMS)*, Oct. 2007, pp. 1999–2003.
[6] G. Lin and X. Sheng, "Application and further development of maglev transportation in China," *Transp. Syst. Technol.*, vol. 4, no. 3, pp. 36–43, 2018.
[7] S. Ren, A. Romeijn, and K. Klap, "Dynamic simulation of the maglev vehicle/guideway system," *J. Bridge Eng.*, vol. 15, no. 3, pp. 269–278, 2009.
[8] Y.-G. Li, W.-S. Chang, and D. Zhang, "The analysis of levitation control system's restriction on the grade ability of EMS maglev," *J.-Nat. Univ. Defense Technol.*, vol. 27, no. 4, p. 106, 2005.
[9] C. F. Zhao, W. M. Zhai, and Q. C. Wang, "Simulation analysis of the dynamic response of low-speed maglev vehicle curve negotiation," *China Railway Sci.*, vol. 26, no. 3, pp. 94–98, 2005.
[10] J. Shi, Q. Wei, and Y. Zhao, "Analysis of dynamic response of the high-speed EMS maglev vehicle/guideway coupling system with random irregularity," *Vehicle Syst. Dyn.*, vol. 45, no. 12, pp. 1077–1095, 2007.

[11] Y. Pei-Chang, L. Jin-hui, L. Jie, and W. Lian-Chun, "Influence of track periodical irregularities to the suspension system of low-speed maglev vehicle," in *Proc. 34th Chin. Control Conf. (CCC)*, Jul. 2015, pp. 8479–8484.
[12] H. K. Sung, J.-M. Jho, D.-K. Bae, K.-S. Rho, J. M. Lee, M.-H. Yoo, and Y.-Y. Nam, "A fuzzy based treatment to reduce air-gap disturbance at the rail joints with step-wise rail joint," in *Proc. 19th Int. Conf. Magn. Levitated Syst. Linear Drives (MAGLEV)*. Dresden, Germany: Technische Univ. Dresden, 2006, p. 4. [Online]. Available: https://trid.trb.org/view/795654
[13] K. Lin, S. Lei, and L. She, "Algorithm on maglev system running across railway step," *Ordnance Ind. Automat.*, to be published.
[14] Y. Zhai and J. Wu, "Algorithm for gap compensating signal of maglev levitation sensor to suppress disturbance from guide way step," *J. China Railway Soc.*, vol. 38, no. 7, pp. 77–83, 2016.
[15] S. Zhou, J. Li, and Y. Li, "Research of algorithm for railway step compensation of mid-low speed maglev," in *Proc. Chin. Automat. Congr. (CAC)*, Oct. 2017, pp. 1276–1280.
[16] K. Zhang, P. Cui, and J. Li, "Accelerometer feedback control algorithm for maglev system," *Control Theory Appl.*, vol. 26, no. 9, pp. 988–992, 2009.
[17] F. Zhou, "Research on levitation control considering some guideway factors," M.S. thesis, Nat. Univ. Defense Technol., Changsha, China, 2009.
[18] H.-K. Liu and X. Zhang, "Maglev control algorithm adapted to variety of track curve," *J. Syst. Simul.*, vol. 22, no. 5, pp. 1101–1105, 2010.
[19] D. Zhou, P. Yu, L. Wang, and J. Li, "An adaptive vibration control method to suppress the vibration of the Maglev train caused by track irregularities," *J. Sound Vib.*, vol. 408, pp. 331–350, Nov. 2017.
[20] Y. Li, P. Yu, D. Zhou, and J. Li, "Magnetic flux feedback strategy to suppress the gap fluctuation of low speed maglev train caused by track steps," in *Proc. 37th Chin. Control Conf. (CCC)*, Jul. 2018, pp. 983–989.
[21] K. Zhang, "Research on digital control technology of MAGLEV vehicle's suspension system," Ph.D. dissertation, Nat. Univ. Defense Technol., Changsha, China, 2004.
[22] G. He, J. Li, and P. Cui, "Decoupling control design for the module suspension control system in maglev train," *Math. Problems Eng.*, vol. 2015, Dec. 2014, Art. no. 865650.
[23] W. Q. Zhang, J. Li, K. Zhang, and P. Cui, "Decoupling suspension controller based on magnetic flux feedback," *Adv. Mater. Res.*, vol. 709, pp. 462–469, Jun. 2013.
[24] Y.-B. Zheng, "Research on decoupling control of EMS type low-mid speed maglev train suspension module," Ph.D. dissertation, National Univ. Defense Technol., Changsha, China, 2006.
[25] K.-W. Lin, "Research on suspension control of low-speed maglev train running on step railway," M.S. thesis, National Univ. Defense Technol., Changsha, China, 2010.
[26] Z.-Y. Jin, S.-Y. Yang, and G.-Z. Ni, "A time-stepping FEM for transient electromagnetic filed analysis and levitation and propellant force study of an EMS maglev train," *Proc. CSEE*, vol. 24, no. 10, pp. 133–137, 2004.
[27] Y.-G. Li, Z.-X. Ke, and H. Cheng, "Analyzing and optimizing design of current-loop in the magnetic levitation controller on maglev vehicle," *J.-Nat. Univ. Defense Technol.*, vol. 28, no. 1, p. 94, 2006.
[28] H. K. Khalil, *Nonlinear Systems*, 3rd ed. Beijing, China: House of Electronics Industry, 2017.
[29] S. Y. Zhang, J. C. Wang, and X. P. Liu, "Differential geometry method and nonlinear control system," *Inf. Control*, vol. 21, no. 5, pp. 288–294, 1992.
[30] C. W. Li and Y. K. Feng, *Inverse System Method for Multivariable Nonlinear Control*. Beijing, China: Tsinghua Univ. Press, 2000.
[31] B. Y. Zhang, "Research on the decoupling control for multivariable nonlinear systems using inverse method," M.S. thesis, Northeastern Univ., Shenyang, China, 2010.
[32] J. D. J. Rubio, "Robust feedback linearization for nonlinear processes control," *ISA Trans.*, vol. 74, pp. 155–164, Mar. 2018.
[33] S.-Z. Chen, F. Lu, Z.-C. Wu, L. Yang, and Y.-Z. Zhao, "Vibration state estimation of nonlinear suspension system based on feedback linearization," *J. Vib. Shock*, vol. 34, no. 20, pp. 10–15, 2015.

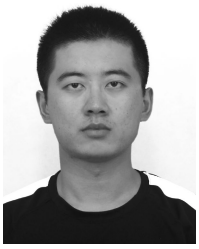

PENG LENG received the B.S. degree in mechanical engineering from Beihang University, Beijing, China, in 2017. He is currently pursuing the M.S. degree with Maglev Engineering Center, National University of Defense Technology, Changsha, China. His current research interests include magnetic levitation control technologies and vehicle-guideway coupling dynamics.

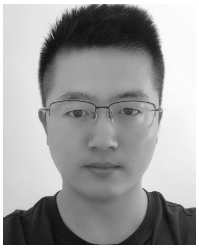

YAJIAN LI received the B.S. and M.S. degrees in automation from the National University of Defense Technology, Changsha, China, in 2013 and 2015, respectively, where he is currently pursuing the Ph.D. degree with Maglev Engineering Center. His current research interests include magnetic levitation control technologies and vehicle-guideway coupling dynamics.

DANFENG ZHOU received the Ph.D. degree in automation from the National University of Defense Technology, Changsha, China, in 2010, where he is currently an Associate Researcher with Maglev Engineering Center. His current research interests include active control of magnetic levitation and maglev vehicle-bridge self-excited vibration.

JIE LI received the Ph.D. degree in automation from the National University of Defense Technology, Changsha, China, in 1999. He held a postdoctoral position with The Hong Kong University of Science and Technology, Hong Kong. He is currently a Professor with Maglev Engineering Center, National University of Defense Technology. His current research interests include magnetic levitation technologies and robotics.

SIYANG ZHOU received the B.S. and M.S. degrees in automation from the National University of Defense Technology, Changsha, China, in 2015 and 2017, respectively. He is currently an Assistant Engineer with the Xichang Satellite Launch Center of China. His current research interests include magnetic levitation control technologies and power electronics technology.